IEEE Photonics Journal
An IEEE Photonics Society Publication

Open Access

Simultaneous Measurement of Pressure and Temperature Based on Adjustable Line Scanning Polarized Low-Coherence Interferometry With Compensation Plate

Volume 10, Number 4, August 2018

Tiegen Liu
Chi Zhang
Shuang Wang
Junfeng Jiang
Kun Liu
Xuezhi Zhang
Xue Wang

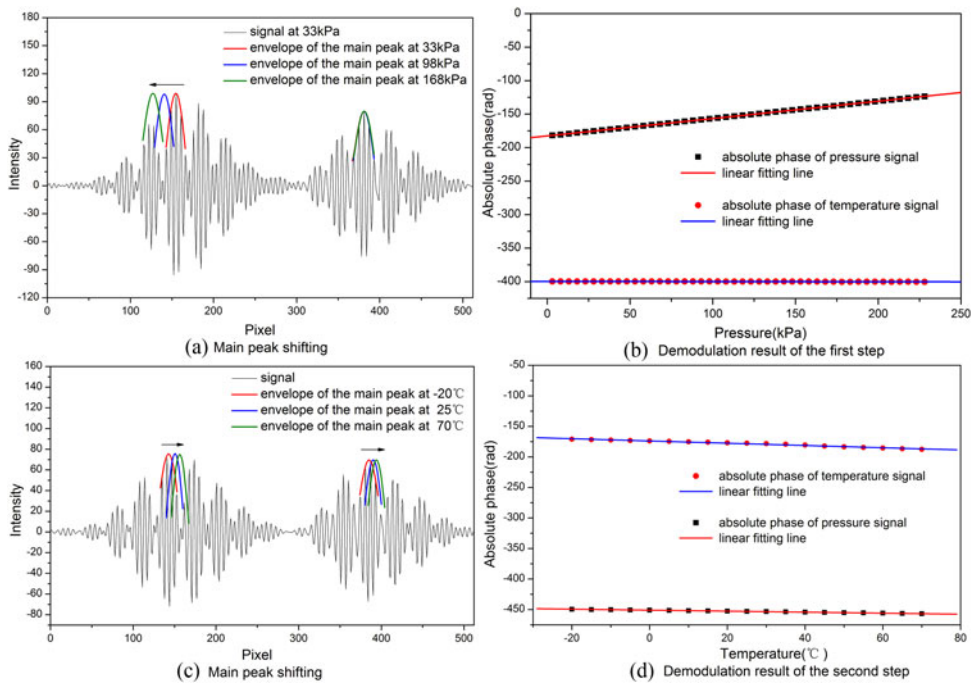

DOI: 10.1109/JPHOT.2018.2856702

Simultaneous Measurement of Pressure and Temperature Based on Adjustable Line Scanning Polarized Low-Coherence Interferometry With Compensation Plate

Tiegen Liu,[1,2,3] **Chi Zhang**,[1,2,3] **Shuang Wang**,[1,2,3] **Junfeng Jiang**,[1,2,3] **Kun Liu**,[1,2,3] **Xuezhi Zhang**,[1,2,3] **and Xue Wang**[1,2,3]

[1]School of Precision Instrument and Opto-Electronics Engineering, Tianjin University, Tianjin 300072, China
[2]Key Laboratory of Opto-Electronics Information Technology, Ministry of Education, Tianjin 300072, China
[3]Tianjin Optical Fiber Sensing Engineering Center, Institute of Optical Fiber Sensing of Tianjin University, Tianjin 300072, China

DOI:10.1109/JPHOT.2018.2856702

Manuscript received May 26, 2018; revised July 10, 2018; accepted July 12, 2018. Date of publication July 18, 2018; date of current version July 26, 2018. This work was supported in part by the National Natural Science Foundation of China under Grants 61505139, 61735011, 61675152, 61475114, and 61378043; in part by the Tianjin Natural Science Foundation under Grant 16JCQNJC02000; in part by the National Instrumentation Program of China under Grant 2013YQ030915; and in part by the China Postdoctoral Science Foundation under Grant 2016M590200. Corresponding authors: Shuang Wang and Junfeng Jiang (e-mail: sarahwang02166@gmail.com; jiangjfjxu@tju.edu.cn).

Abstract: A novel method realized by an adjustable line scanning polarized low-coherence interferometer is proposed and experimentally demonstrated to simultaneously measure pressure and temperature. The combination of birefringence wedge and compensation plate acts as an adjustable line scanning part to adapt various sensors by changing the thickness of compensation plate. The variations of pressure and temperature manifest as shift of the corresponding interference fringes on an infrared line array CCD. The dual-light-source is employed to fix the over occupation of CCD caused by an SLD with longer coherence length than an LED and enlarge the measuring range. An experiment of pressure and temperature was carried out to verify the effectiveness of the proposed method. The experimental results show that the proposed method is appropriate for the simultaneous measurement of pressure and temperature, and the sensor has a good linearity in pressure range of 3–228 kPa and temperature range of −20 °C −70 °C. The measurement errors of the pressure and temperature are less than 0.3%F.S. and 1.1%F.S., respectively.

Index Terms: Fabry-Perot interferometer, optical fiber sensor, dual-light-source, simultaneous pressure and temperature sensing.

1. Introduction

Optical interferometry has been widely researched and applied in various fields, such as biomedicine [1], petrochemical industry [2] and aviation industry [3]. With advantages of high sensitivity, fast response and immunity to electromagnetic interference, the optical interferometry measuring method is extensively employed in sorts of parameters measurement, for instance, temperature [4]–[6],

pressure [7], [8], optical refractive index [9], [10] and strain [11]. Not only for single parameter, the optical interferometry measuring method also suits for dual-parameter simultaneous measurement, such as temperature-refractive index [12], temperature-strain [13], [14] and pressure-temperature [15]–[20].

The simultaneous measurement of pressure and temperature is one of the most valuable research directions because of its broad range of applications. So far, more and more structures have been proposed on pressure-temperature sensing, such as polymer [15], all-fiber or all silica [16], [17], optical fiber Bragg Gratings [18], [19] and PCF [20]. A FBG structure with polymer coating [17] can achieve 2.5%F.S. and 0.6%F.S. precision in pressure and temperature measurement respectively. A kind of all silica sensor [19] have precisions of 1.4%F.S. and 1.6%F.S. Recently, focusing on the broadening and shift rates induced by noble gases and the temperature dependence of the collisional effect, a paper research in pressure and temperature is proposed [21]. However, the aforementioned methods all focus on the spectrum signal. The demodulation efficiency and resolution are limited by the performance of spectrograph. Volume and cost of spectrograph are also problems for application. As an important method to realize optical interference sensing with the advantages of high precision demodulation, compact and economical, the polarized low-coherence interferometry (PLCI) [22] is less discussed in the dual-parameter field.

Different from the spectrum method, PLCI needs to match the optical path difference (OPD) via a birefringence wedge. To satisfy various measurement requirements, the OPD of Fabry-Perot (F-P) sensors are usually different, which will lead to redundant configuration of birefringence wedge for each sensor. Moreover, for common white light PLCI, the coherence length is short [23]. However, in consideration of long distance transmission, a much powerful light source, for example, the superluminescent light-emitting diodes (SLD), should be used to maintain the interference intensity. The accompany problem is the broader envelope of interference signal caused by SLD with longer coherence length than LED [24], [25]. On one hand, this problem limits the shifting scope of the interference fringe and makes simultaneous measurement difficult. On the other hand, it leads to misjudgment of the larger intensity between two adjacent pixels especially near the peak and reduces the demodulation precision.

In this paper, we proposed and experimentally demonstrated a method based on line scanning PLCI for simultaneous measurement of pressure and temperature. The birefringence wedge with compensation plate as the line scanning part make the OPD can be adjusted according to different sensors. The dual-light-source configuration successfully solves simultaneity problems. The compressed signal reduces the occupied space in pixel limited CCD to enlarge the measuring range. The pressure and temperature experiment results show that the system is appropriated to measure the pressure and temperature simultaneously. In the pressure range 3–228 kPa and temperature range −20–70 °C, the sensor has a good linearity, and the pressure and temperature measurement errors are less than 0.3%F.S. and 1.1%F.S. respectively.

2. Principle Analyze

2.1 System Principle

Fig. 1. is a simplified diagram of dual-parameter PLCI system. Two beams from two SLDs with different central wavelengths converge into one with both wave bands in the first 3 dB coupler. The converging beam has a broader wave band and transmits into a dual-parameter F-P sensor via the second 3 dB coupler module. The reflected light with OPD caused by sensor is led to the PLCI demodulation module via the second 3 dB coupler. In the PLCI demodulation module, the light go through a cylindrical lens, a convex, a polarizer, a birefringence wedge part covered by compensation plate, and an analyzer. The birefringence wedge and the compensation plate add an OPD between ordinary (O) ray and extraordinary (E) ray. The interference fringe will only appear on the infrared 1-dimension linear array CCD camera where the OPD produced by birefringence wedge and the compensation plate is equal to the corresponding OPD produced by sensor.

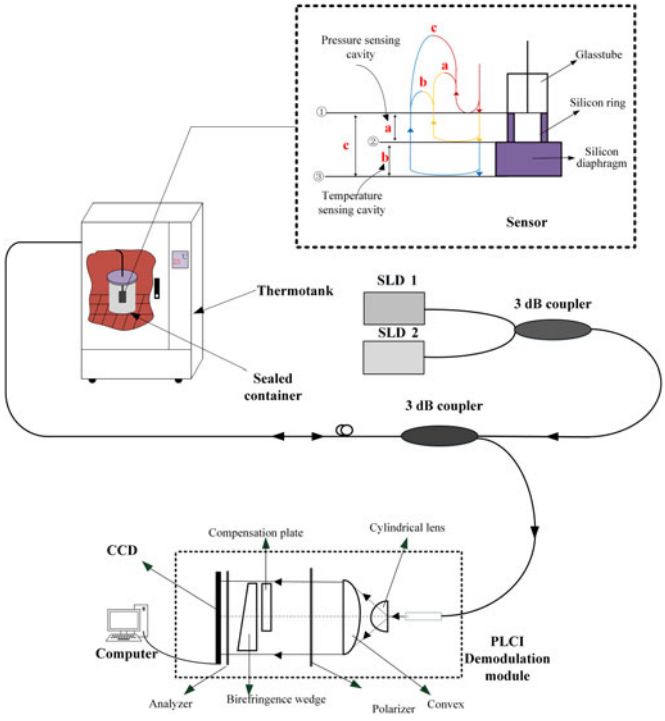

Fig. 1. Simplified diagram of dual-parameter PLCI system.

2.2 Sensor, Birefringence Wedge, and Compensation Plate

As three main components of the dual-parameter F-P sensor, a silicon circular ring is sandwiched between a thin silicon circular diaphragm and a glass tube with a capillary interstice through it, as shown in Fig. 1. After the incidence of the converge beam, there are three different intensities of light reflected by three different reflecting surfaces, the end surface of the optical fiber ①, the front and back surfaces of the silicon diaphragm ②, ③. These three reflected light will generate composite interference (a, b, and c). Focusing on the OPD that make interference happen, we can clearly see that there will be three distinct OPDs forming three lengths of F-P cavity. For a, the OPD is twice the optical path length between reflecting surface ① and ②, and a corresponds to the air cavity. Similarly, b and c correspond to the silicon cavity and the composite cavity, respectively. We choose the air cavity and the silicon cavity as our measurement units. The OPD of air cavity is simultaneously influenced by both pressure and temperature, and the OPD of silicon cavity is temperature dependent only. When the pressure and temperature in the environment change, the variation of two OPDs generated by air and silicon F-P cavity can be expressed as the equations:

$$\Delta_P = 2h_a - 2S_p dP + 2S_g dT \tag{1}$$

$$\Delta_T = 2(n + \xi dT)(1 + \varepsilon dT)h_b \tag{2}$$

where Δ_P and Δ_T represent the OPD of the air F-P cavity and the silicon F-P cavity, respectively. dP and dT represent the variation of the pressure and the temperature, respectively. h_a and h_b represent the original geometry length of a and b in Fig. 1, respectively. ε, ξ and n represent the thermal expansion coefficient, the thermal optical coefficient, and the refractive index of the silicon diaphragm, respectively. $S_p = 3r^4(1-\upsilon^2)/(16Et^3)$ is the pressure sensitivity of the silicon diaphragm, where r is the radius of the air F-P cavity, t, E and υ represent the thickness, Young's modulus and the Poisson ratio of the silicon diaphragm, respectively. $S_g = S_p P_0 / T_0$ is the temperature sensitivity arise from residual air in the F-P cavity, where $T_0 = 298\ K$ is normal temperature, P_0 is the residual pressure

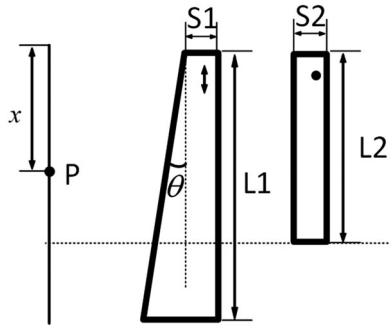

Fig. 2. Birefringence wedge and compensation plate make appropriate OPD range for dual-parameters measurement.

in the cavity at T_0. In our paper, the sensor has a pressure sensing cavity made of $\sim$25 μm thick air and a temperature sensing cavity made of $\sim$45 μm thick silicon diaphragm.

The birefringence wedge and compensation plate split the CCD into two different parts which corresponds to pressure and temperature interference fringe respectively, as shown in Fig. 2. The birefringence wedge and compensation plate with orthogonal optical axes are made of same birefringent crystal which can make the OPD range for scanning more adjustable. In the meantime, the OPD is related with the angle and the length of the birefringence wedge. Taking the birefringence wedge as the positive direction, the geometric optical path d generated by birefringence wedge and compensation plate for any point P on CCD can be expressed as the following equation:

$$d = \begin{cases} x \cdot \mu \cdot \tan\theta + S1 - S2 & 0 < L \leq L2 \\ x \cdot \mu \cdot \tan\theta + S1 & L2 < L < L1 \end{cases} \tag{3}$$

where x is the corresponding pixel number on the CCD, μ is the interval between two pixels on the CCD, θ is the angle of the birefringence wedge, $S1$, $S2$, $L1$, $L2$ is the thickness and length of the birefringence wedge and compensation plate, respectively. The corresponding OPD can be calculated by multiplying geometric optical path d by refractive index difference between the O ray and the E ray. From the equation (3), line scanning distribution is built in both with- and without-compensation plate parts. To ensure a single frame of the signal only have the interference fringe of pressure and temperature at each part, the OPD range that produced by each part should cover the OPD produced by air cavity and the silicon cavity, respectively, and the OPD made by composite cavity won't have corresponding position in both parts. When the OPD produced by sensor changes linearly, the associated interference fringe shifts on the CCD linearly. With a same birefringence wedge, changing the thickness of the compensation plate $S2$ can make the demodulation module adapt different measuring ranges, and changing the length of the compensation plate $L2$ can make various distribution ratios of two parts.

2.3 Dual-Light-Source and Demodulation With Dispersion

In order to get long distance sensing, we use two SLDs with different central wavelengths as the system light source. The attendant problem is the long coherence length caused by single SLD. Moreover, a broader interference envelope makes it hard to identify the peak value while environment noise is big enough, which will influence the demodulation results. Considering of the pixel limited CCD and the demodulation precision, it is essential to shorten the coherence length of the interference fringe. Meanwhile, a narrower interference envelope is in favor of expanding the measurement range. One effective method is employing dual-light-source. The interference fringe generated by single-light-source and dual-light-source is simulated in Fig. 3. Since light source have broader wave band, the birefringence dispersion factor should be taken into account in our simulation. An interference fringe generated by single light source can be regarded as an

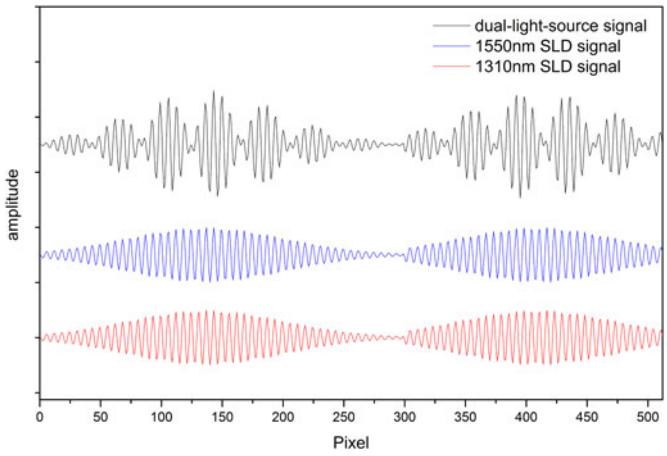

Fig. 3. Simulation of dual-light-source system.

approximate double-beam interference which can be expressed as [26]:

$$I(d, h, k_0, \Delta k) = (1+\eta^2)^{-1/4} \exp\left[-\frac{(z\Delta k)^2}{4\gamma(1+\eta^2)}\right] \cos\left[\Phi(d, h, k_0, \Delta k)\right] \tag{4}$$

$$\Phi(d, h, k_0, \Delta k) = zk_0 - \alpha k_0^2 d + 1/2 \arctan\eta - \frac{\eta \Delta k^2 z^2}{4\gamma(1+\eta^2)} \tag{5}$$

where I represents the interference fringe intensity using a single light source, $\gamma = 4\ln 2$, $\eta = \alpha\Delta k^2 d/\gamma$, $z = N(k_0)d - 2h$, $N(k_0) = n(k_0) + \alpha k_0$, α is the birefringence dispersion slope of the birefringence wedge material, h is corresponding F-P cavity length, $n(k_0)$ is the birefringent crystal's refractive index difference between the O ray and the E ray while the wave number is the central wave number k_0, $k_0 = 2\pi/\lambda_0$, λ_0 is the central wavelength, $\Delta k = 2\pi\Delta\lambda/\lambda^2$, where $\Delta\lambda$ is the FWHM of the power spectrum in the wavelength domain.

When it comes to dual-light-source, the interference fringe's intensity can be considered as coherent superposition of two interference fringes generated by each light source.

$$I_d = I_1(d, h, k_1, \Delta k_1) + I_2(d, h, k_2, \Delta k_2) \tag{6}$$

where I_d represents the interference fringe intensity for dual-light-source, I_1 and I_2 are the interference fringe intensity for different single light sources, respectively.

The following parameter setting is as same as the experiment in this paper: $n(k_1) = 0.1199$, $n(k_2) = 0.1202$, $\alpha = 0.00125$, $\theta = 4^\circ$, $h1 = 25\mu$m, $h2 = 157\mu$m, $\mu = 25\ \mu$m, $\lambda_1 = 1310$ nm, $\lambda_2 = 1550$ nm, $\Delta\lambda_1 = 40$ nm, $\Delta\lambda_2 = 70$ nm, $S1 = S2 = 1.5$ mm, $L1 = 20$ mm, $L2 = 12$ mm. x ranges from 1 to 512 as the CCD pixel number. The OPDs generated by birefringence wedge with or without compensation plate can be calculated as 0∼100.5 and 280.8∼347.8. So each of the OPDs generated by sensor can be found in two different OPD ranges provided by birefringence wedge and compensation plate. Therefore, two interference fringes are both visible. We keep the intensity of both light sources at ∼9 mW to maintain the status that they are approximately 1:1. The simulation result is shown in Fig. 3.

From Fig. 3, we can see the envelope is much narrower when using dual-light-source which is essential to enlarge the measurement range. Using dual-light-source configuration, we can arrange two interference fringes together in one frame of CCD, and avoid the overlap of them. With matching parameters of birefringence wedge and compensation plate, we can measure the pressure and temperature simultaneously.

For each frame of signal under different environment, we first split the signal into two parts. Each part includes an interference fringe. For each part, we deploy a monochromatic frequency

TABLE 1
Information of the Birefringence Wedge and the Compensation Plate

Birefringence wedge	Short side width S1	1.5mm
	Wedge angle θ	4°
	Length L1	20mm
Compensation plate	Length L2	12mm
	Length S2	1.5mm

TABLE 2
Light Sources Parameter Contract

	SLD1	SLD2
Central wavelength/nm	1310	1550
Bandwidth/nm	40	70
Intensity/mW	9.09	9.00

absolute phase demodulation method with filtering window and compensation for frequency domain nonlinearity induced by birefringence dispersion to get the absolute phase Φ of each interference fringe [27], [28]. Meanwhile, the OPD of F-P cavity length Δ has a linear relationship with variation of absolute phase $\Delta\Phi$ according to formula [22]:

$$\Delta = \frac{\lambda_u}{2\pi} \cdot \Delta\Phi \tag{7}$$

where λ_u is the wavelength used in demodulation to unwrap the phase. We can relate the variations of absolute phase and the pressure or temperature from equation (1), (2), and (7).

3. Experiment and Discussion

The pressure and temperature experiment was carried out to verify the feasibility and performance of the proposed method. The schematic diagram of the experiment system is shown in Fig. 1.

A sealed container is used to create the pressure condition we need. The pressure could be controlled by an external pressure source with accuracy of 0.02 kPa. The container with the dual-parameter F-P sensor is put into a thermostat to provide temperature changes with precision of 0.1 °C. The information of the birefringence wedge and the compensation plate is listed in the Table 1, the light sources parameter contract is listed in Table 2:

The received signal of sensor is shown in Fig. 4.

The ravine at ~300 pixel is formed by the edge of the compensation plate. The pressure interference fringe and temperature interference fringe lies on the left and right of the ravine, respectively.

We split the experiment into two parts. On one hand, we maintain the room temperature (25 °C) and increase the pressure from 3 kPa to 228 kPa. Because of the constant temperature, thermal expansion of residual gas and silicon and thermal optical effect of silicon can be neglected. Since the pressure rising, defromation of silicon diaphragm reduces the OPD generated by air cavity, so the pressure interference fringe shifts to the left while the temperature one keeps still, as shown in Fig. 5(a). The shift tendencies of two interference fringes in accordance with the changing of the each parameter. We set the pressure interval 5 kPa during the experiment. The absolute phase-pressure and absolute phase-temperature curves are shown in Fig. 5(b). The pressure sensitivity of pressure interference fringe and temperature interference fringe signal can be calculated as $2.592 * 10^{-1}$ rad/kPa and $6.25 * 10^{-4}$ rad/kPa. The measurement error of the pressure is shown in Fig. 6(a), which is less than 0.3%F.S. On the other hand, we keep the pressure 101 kPa and increase the temperature from −20 °C to 70 °C. The temperature interference fringe shifts to the right

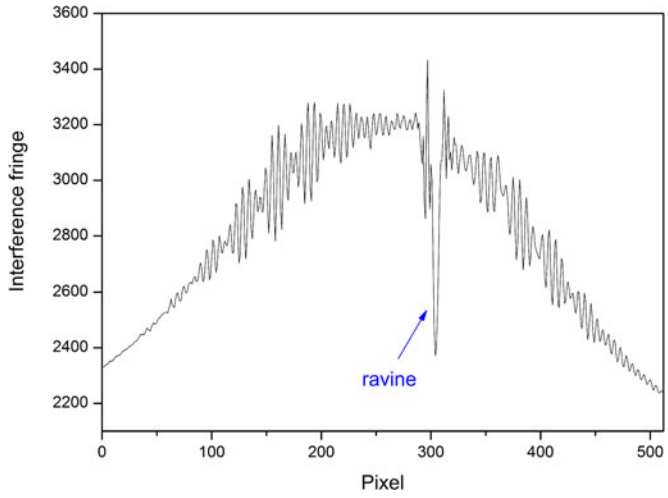

Fig. 4. Signal received on the CCD.

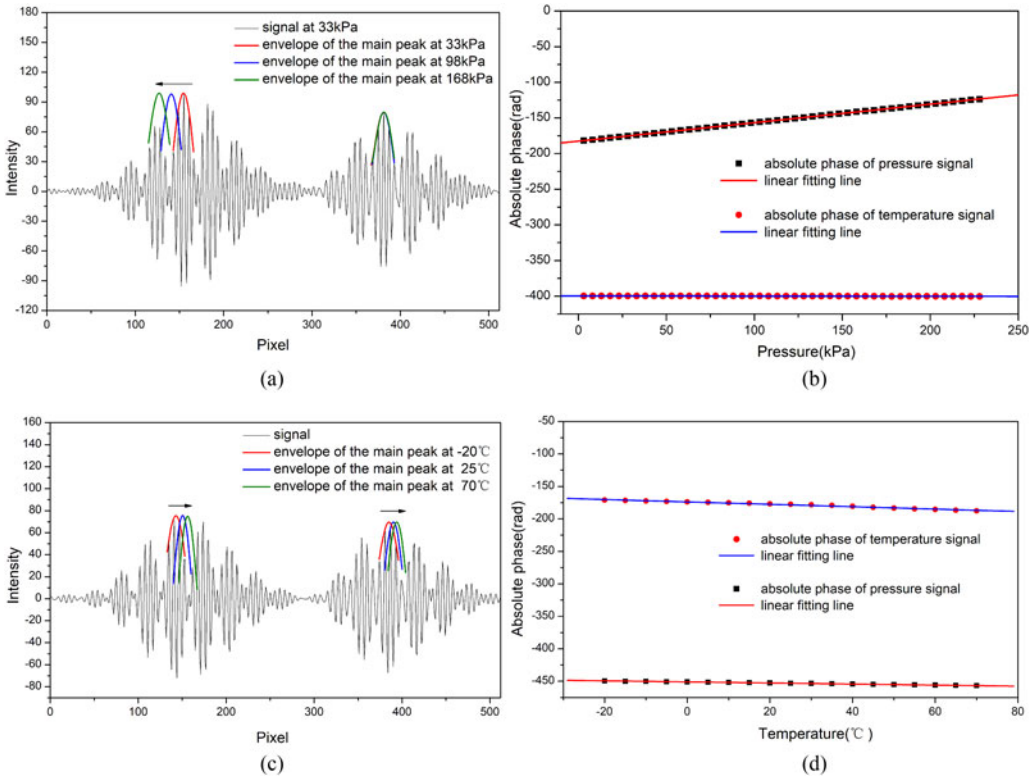

Fig. 5. Results of experiment. (a) Main peak shifting. (b) Demodulation result of the first step. (c) Main peak shiting. (c) Demodulation result of the second step.

direction. Since the residential gas in the air cavity expands with heat, the pressure interference fringe also shifts to the right direction as shown in Fig. 5(c). The absolute phase-pressure and absolute phase-temperature curve are shown in Fig. 5(d). The temperature sensitivity of pressure interference fringe and temperature interference fringe signal can be calculated as 0.18 rad/ °C and 0.08 rad/ °C. The measurement error of the temperature is shown in Fig. 6(b), which is less than

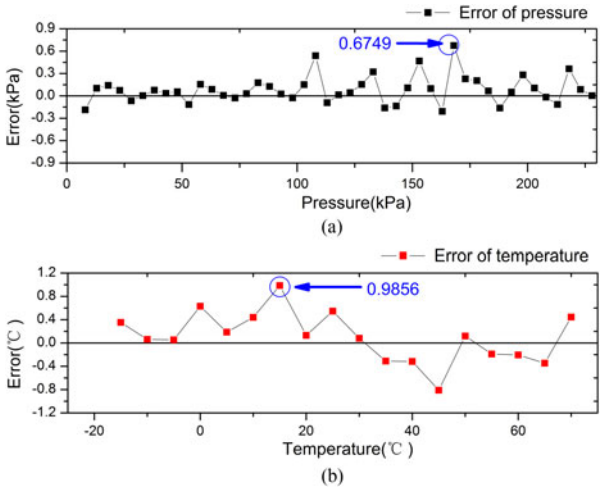

Fig. 6. Measurement error. (a) Pressure measurement error. (b) Temperature measurement error.

1.1%F.S. The demodulation matrix of the sensor is expressed as following formula:

$$\begin{bmatrix} \Delta\Phi_{FP1} \\ \Delta\Phi_{FP2} \end{bmatrix} = \begin{bmatrix} 0.26 & 0.18 \\ 0.000625 & 0.08 \end{bmatrix} \begin{bmatrix} dP \\ dT \end{bmatrix} \tag{8}$$

where $\Delta\Phi_{FP1}$ and $\Delta\Phi_{FP2}$ are in the unit of rad, while dP and dT are in the units of kPa and °C respectively. By solving this equation, the pressure and temperature can be calculated simultaneously by

$$\begin{bmatrix} dP \\ dT \end{bmatrix} = \begin{bmatrix} 4.02 & -9.05 \\ -0.03 & 12.57 \end{bmatrix} \begin{bmatrix} \Delta\Phi_{FP1} \\ \Delta\Phi_{FP2} \end{bmatrix} \tag{9}$$

4. Conclusion

In this paper, we proposed a method for simultaneous measurement of pressure and temperature based on adjustable line scanning PLCI. The dual-light-source configuration successfully enlarges the measuring range and solves simultaneity problems. The birefringence wedge with compensation plate as the line scanning part could handle a large range of sensor's different F-P cavity lengths. The pressure and temperature experiment results show a good linearity of the sensor for both pressure and temperature. The method is appropriate to measure the pressure and temperature simultaneously with the F-P sensor in the range from 3 kPa to 228 kPa pressure condition and −20 °C to 70 °C temperature condition.

References

[1] F. Zhang *et al.*, "Flexible and self-powered temperature-pressure dual-parameter sensors using microstructure-frame-supported organic thermoelectric materials," *Nat. Commun.*, vol. 6, 2015, Art. no. 8356.
[2] G. R. Pickrell *et al.*, "Fiber optic pressure and temperature sensors for oil down hole application," *Sci. Technol. Eng.*, vol. 4578, pp. 182–190, 2010.
[3] Z. P. Zhou, H. L. Shan, J. I. Dong-Dong, and C. F. Ding, "Development of a high temperature fiber optic cable for aviation," *Electric Wire Cable*, 2016.
[4] Y. Lu and M. Han, "Fiber-optic temperature sensor using dual Fabry–Perot cavities filled with gas of different pressure," *Sens. Actuators A. Phys.*, vol. 261, pp. 229–234, 2017.
[5] H. Y. Choi, K. S. Park, S. J. Park, U. C. Paek, B. H. Lee, and E. S. Choi, "Miniature fiber-optic high temperature sensor based on a hybrid structured Fabry–Perot interferometer," *Opt. Lett.*, vol. 33, no. 21, pp. 2455–2457, 2008.
[6] T. Liu, J. Yin, J. Jiang, K. Liu, S. Wang, and S. Zou, "Differential-pressure-based fiber-optic temperature sensor using Fabry–Perot interferometry," *Opt. Lett.*, vol. 40, no. 6, pp. 1049–1052, 2015.

[7] Y. Zhang, L. Yuan, X. Lan, A. Kaur, J. Huang, and H. Xiao, "High-temperature fiber-optic Fabry–Perot interferometric pressure sensor fabricated by femtosecond laser," *Opt. Lett.*, vol. 38, no. 22, pp. 4609–4612, 2013.
[8] X. Wang *et al.*, "Non-destructive residual pressure self-measurement method for the sensing chip of optical Fabry-Perot pressure sensor," *Opt. Exp.*, vol. 25, no. 25, pp. 31937–31947, 2017.
[9] P. Jia *et al.*, "Temperature-compensated fiber-optic Fabry–Perot interferometric gas refractive-index sensor based on hollow silica tube for high-temperature application," *Sens. Actuators B, Chem.*, vol. 244, pp. 226–232, 2017.
[10] Z. Ran, Y. Rao, J. Zhang, Z. Liu, and B. Xu, "A miniature fiber-optic refractive-index sensor based on laser-machined Fabry–Perot interferometer tip," *J. Lightw. Technol.*, vol. 27, no. 23, pp. 5426–5429, Dec. 2009.
[11] G. D. Peng, J. Zhang, L. Yuan, and W. Sun, "Composite-cavity-based Fabry–Perot interferometric strain sensors," *Opt. Lett.*, vol. 32, no. 13, pp. 1933–1935, 2007.
[12] D. W. Kim *et al.*, "Simultaneous measurement of refractive index and temperature based on a reflection-mode long-period grating and an intrinsic Fabry–Perot interferometer sensor," *Opt. Lett.*, vol. 30, no. 22, pp. 3000–3002, 2005.
[13] A. Zhou *et al.*, "Hybrid structured fiber-optic Fabry–Perot interferometer for simultaneous measurement of strain and temperature," *Opt. Lett.*, vol. 39, no. 18, pp. 5267–5270, 2014.
[14] T. Liu, G. F. Fernando, Z. Y. Zhang, and K. T. V. Grattan, "Simultaneous strain and temperature measurements in composites using extrinsic Fabry–Perot interferometric and intrinsic rare-earth doped fiber sensors," *Sens. Actuators A, Phys.*, vol. 80, no. 3, pp. 208–215, 2000.
[15] H. Bae, D. Yun, H. Liu, D. A. Olson, and M. Yu, "Hybrid miniature Fabry–Perot sensor with dual optical cavities for simultaneous pressure and temperature measurements," *J. Lightw. Technol.*, vol. 32, no. 8, pp. 1585–1593, Apr. 2014.
[16] D. H. Wang, L. Y. Zeng, P. G. Jia, L. Liu, and X. Y. Jiang, "Simultaneous measurement of acoustic pressure and temperature in the HIFU fields using all-silica fiber optic Fabry-Perot hydorophone," *Proc. SPIE—Int. Soc. Opt. Eng.*, vol. 9274, 2014, Art. no. 92740T.
[17] A. Sun *et al.*, "Study of simultaneous measurement of temperature and pressure using double fiber Bragg gratings with polymer package," *Opt. Eng.*, vol. 85, no. 44, pp. 4831–4834, 2005.
[18] N. Dong *et al.*, "Pressure and temperature sensor based on graphene diaphragm and fiber Bragg gratings," *IEEE Photon. Technol. Lett.*, vol. 30, no. 5, pp. 431–434, Mar. 2018.
[19] S. Pevec and D. Donlagic, "Miniature all-fiber Fabry–Perot sensor for simultaneous measurement of pressure and temperature," *Appl. Opt.*, vol. 51, no. 19, pp. 4536–4541, 2012.
[20] M. M. Ali, R. Islam, K. Lim, and D. S. Gunawardena, "PCF-cavity FBG Fabry–Perot resonator for simultaneous measurement of pressure and temperature," *IEEE Sensors J.*, vol. 15, no. 12, pp. 6921–6925, Dec. 2015.
[21] R. Li *et al.*, "Pressure broadening and shift of K D 1, and D 2, lines in the presence of 3 He and 21 Ne," *Eur. Phys. J. D*, vol. 70, no. 6, 2016, Art. no. 139.
[22] J. Jiang *et al.*, "A polarized low-coherence interferometry demodulation algorithm by recovering the absolute phase of a selected monochromatic frequency, " *Opt. Exp.*, vol. 20, no. 16, pp. 18117–18126, 2012.
[23] A. W. Palmer *et al.*, "Digital signal-processing techniques for electronically scanned optical-fiber white-light interferometry," *Appl. Opt.*, vol. 31, no. 28, pp. 6003–6010, 1992.
[24] Y. Rao, Y. Ning, and D. A. Jackson, "Synthesized source for white light sensing system," *Opt. Lett.*, vol. 18, no. 6, pp. 462–464, 1993.
[25] S. Chen *et al.*, "Instantaneous fringe-order identification using dual broadband sources with widely spaced wavelengths," *Electron. Lett.*, vol. 29, no. 4, pp. 334–335, 2002.
[26] S. Wang *et al.*, "Birefringence dispersion compensation demodulation algorithm for polarized low-coherence interferometry," *Opt. Lett.*, vol. 38, no. 16, pp. 3169–3172, 2013.
[27] S. Wang *et al.*, "Birefringence-dispersion-induced frequency domain nonlinearity compensation for polarized low-coherence interferometry demodulation," *J. Lightw. Technol.*, vol. 33, no. 23, pp. 4842–4848, 2015.
[28] K. Liu *et al.*, "An improved optical fiber remote sensing method based on polarized low-coherence interferometry," *IEEE Photon. J.*, vol. 10, no. 1, Feb. 2018, Art. no. 6800409.